The HIF-pathway inhibitor NSC-134754 induces metabolic changes and anti-tumour activity while maintaining vascular function

LCJ Baker*[,1], JKR Boult[1], S Walker-Samuel[1,2], Y-L Chung[1], Y Jamin[1], M Ashcroft[3] and SP Robinson[1]

[1]Cancer Research UK and EPSRC Cancer Imaging Centre, Division of Radiotherapy and Imaging, The Institute of Cancer Research and Royal Marsden NHS Trust, 15 Cotswold Road, Belmont, Sutton, Surrey SM2 5NG, UK; [2]Division of Medicine and Institute of Child Health, Centre for Advanced Biomedical Imaging, University College London, 72 Huntley Street, London WC1E 6DD, UK; [3]Division of Medicine, Centre for Cell Signalling and Molecular Genetics, University College London, Rayne Building, 5 University Street, London WC1E 6JF, UK

BACKGROUND: Hypoxia-inducible factor-1 (HIF-1) mediates the transcriptional response to hypoxic stress, promoting tumour progression and survival. This study investigated the acute effects of the small-molecule HIF-pathway inhibitor NSC-134754.

METHODS: Human PC-3LN5 prostate cancer cells were treated with NSC-134754 for 24 h in hypoxia. Orthotopic prostate tumour-bearing mice were treated with a single dose of NSC-134754 for 6, 24 or 48 h. Treatment response was measured using magnetic resonance spectroscopy and imaging. Ex-vivo histological validation of imaging findings was also sought.

RESULTS: In vitro, NSC-134754 significantly reduced lactate production and glucose uptake ($P < 0.05$), while significantly increasing intracellular glucose ($P < 0.01$) and glutamine uptake/metabolism ($P < 0.05$). Increased glutamine metabolism was independent of c-Myc, a factor also downregulated by NSC-134754. In vivo, a significantly higher tumour apparent diffusion coefficient was determined 24 h post-treatment ($P < 0.05$), with significantly higher tumour necrosis after 48 h ($P < 0.05$). NSC-134754-treated tumours revealed lower expression of HIF-1α and glucose transporter-1, at 6 and 24 h respectively, while a transient increase in tumour hypoxia was observed after 24 h. Vessel perfusion/flow and vascular endothelial growth factor levels were unchanged with treatment.

CONCLUSION: NSC-134754 induces metabolic alterations in vitro and early anti-tumour activity in vivo, independent of changes in vascular function. Our data support the further evaluation of NSC-134754 as an anti-cancer agent.

Solid tumours typically exhibit hypoxic regions that are associated with a more aggressive phenotype, impacting negatively on treatment response and patient survival (Gray et al, 1953; Vaupel et al, 2004; Tatum et al, 2006). A key mediator of hypoxic cell survival and adaptation is the hypoxia-inducible factor-1 (HIF-1) pathway (Semenza, 2000). Hypoxia-inducible factor-1 is a hetero-dimeric transcription factor composed of the oxygen-labile HIF-1α, and constitutively expressed HIF-1β subunits. In response to hypoxia, HIF-1α is stabilised allowing dimerisation with HIF-1β to form the HIF-1 complex (Wang and Semenza, 1995). Translocation of HIF-1 to the nucleus and binding to hypoxic response elements leads to the transcription and translation of numerous genes (Semenza et al, 1994; Carmeliet et al, 1998; Pugh and Ratcliffe, 2003). Importantly, many of the upregulated genes have recognised functions in tumourigenesis, modulating tumour metabolism, and enhancing angiogenesis, invasion and metastasis (Maxwell et al, 1997; Semenza, 2003; Robey et al, 2005). Given the diversity of the pathogenic pathways involved, compounds that target HIF-1 or components of the HIF pathway are actively being sought, and several small-molecule inhibitors of the HIF pathway are currently in clinical trials (Onnis et al, 2009; Tennant et al, 2010).

To assist in the evaluation of novel HIF inhibitors, reliable, reproducible and informative biomarkers capable of assessing tumour response are required. Magnetic resonance imaging (MRI) is one non-invasive technique used clinically to investigate tumour response to a wide range of cancer therapeutics. Conventionally, the response evaluation criteria in solid tumours (RECIST) imaging criteria denotes the assessment of tumour volume in response to various interventions over time. However, evidence is emerging that novel targeted therapeutics may elicit efficacy before any reduction in tumour volume, and that the measurement of acute functional changes in tumour pathophysiology in vivo may be more revealing (Michaelis and Ratain, 2006). In this regard, functional imaging techniques such as dynamic contrast-enhanced MRI (DCE-MRI), which reports on tumour vascular permeability/perfusion, and diffusion-weighted MRI (DW-MRI), used to assess tissue cellularity and necrosis, are being extensively used to evaluate tumour therapeutic response in both pre-clinical and clinical trials (Leach et al, 2005; Padhani et al, 2009). In addition,

---

magnetic resonance spectroscopy (MRS) can provide a quantitative snapshot of cellular metabolism, allowing an insight into therapy-induced shifts in energy pathways and metabolic consumption (Griffiths et al, 2002; Beloueche-Babari et al, 2010). The use of MRI/MRS to investigate novel pharmacological HIF inhibitors, and with it increase understanding and context of potential clinical application, is gaining momentum (Jordan et al, 2005a; Jordan et al, 2005b).

In this study, we have used several MR techniques to investigate acute response of human prostate cancer cells to the HIF-pathway inhibitor NSC-134754 in vitro, and in a murine orthotopic prostate model in vivo. NSC-134754 was previously identified from a cell-based screening assay as a translational inhibitor of HIF-1 in response to both hypoxic stress and growth-factor-mediated pathways (Chau et al, 2005). In vivo, NSC-134754 has demonstrated preclinical anti-tumour activity in a mouse model of human glioblastoma, inducing tumour shrinkage post-irradiation during a 3-week treatment regime, with continued shrinkage observed post-treatment until experiment end (Kioi et al, 2010). Treatment response to NSC-134754 in human prostate carcinoma has not yet been reported. We demonstrate the utility of MRS and MRI in assessing the metabolic effects of HIF-pathway inhibition with NSC-134754 in human prostate cells in vitro, and acute functional changes in orthotopic prostate xenografts in vivo. Complementary techniques to validate the activity of NSC-134754 were also sought, including effects on cellular proliferation and expression of HIF-1α and the downstream targets vascular endothelial growth factor (VEGF) and glucose transporter-1 (GLUT-1). Additionally, changes in the tumour microenvironment induced by NSC-134754 on tumour perfusion, hypoxia and necrosis were also investigated.

MATERIALS AND METHODS

Cell culture and hypoxic conditions

Human PC-3LN5 prostate tumour cells were a kind gift from Dr S Eccles (Cancer Therapeutics Unit, Institute of Cancer Research). These cells were originally generated in-house from the lymph node metastases of orthotopic PC-3 tumours grown in male NCr nude mice (Sanderson et al, 2006). Cells were maintained in RPMI 1640 media supplemented with 10% (v/v) fetal bovine serum (Gibco by Invitrogen, Paisley, UK) at 37 °C in a humidified incubator with an atmosphere of 5% CO_2 in 95% air. In-vitro experiments were performed under hypoxia, with cells plated and allowed to adhere in normoxic conditions before incubation in a humidified hypoxic workstation (Hypoxystation, Don Whitley Scientific, Shipley, UK), pre-equilibrated to 1.0% O_2, 5% CO_2.

Drug preparation

NSC-134754 was obtained from the National Cancer Institute's Developmental Therapeutics Program (MD, USA). For in-vitro experiments, dilutions were prepared in culture medium on the day of the experiment from frozen 1 mM stock. For in-vivo experiments, 30 mg ml^{-1} NSC-134754 was freshly prepared in 0.9% NaCl before intraperitoneal injection.

Sulforhodamine B assay

The sulforhodamine B assay was performed to measure the effects of NSC-134754 on cell proliferation and establish the GI$_{50}$ inhibition of cell growth (the concentration needed to reduce the growth of treated cells to half that of untreated cells). Cells were incubated in 100 μl medium in 96-well plates (Corning Incorporated, Corning, NY, USA) for 48 h before the addition of 100 μl drug-containing medium. Final concentrations of NSC-134754 ranged from 0.0012 to 10 μM in a final volume of 200 μl. Fixation and staining followed the standard method developed by Skehan et al (1990).

Western blot analysis

Whole cell lysates were prepared and analysed for western blotting as described previously (Bardos and Ashcroft, 2004). A minor modification included harvesting cells in RIPA buffer (Cell Signaling, Boston, MA, USA) supplemented with 1 × complete protease inhibitor (Roche Applied Sciences, Burgess Hill, UK) for protein determination and GLUT-1, LDH-A and c-Myc analysis. Antibodies used included anti-human HIF-1α (clone 54, BD Transduction Laboratories, Lexington, KY, USA, 1 : 500), anti-human GLUT-1 (Millipore, Billerica, MA, USA, 1 : 100), anti-human LDH-A (Santa Cruz Biotechnology, Santa Cruz, CA, USA, 1 : 3000) and anti-c-Myc (Cell Signaling, 1 : 3000). β-Actin (GE Healthcare, Buckinghamshire, UK, 1 : 5000) was detected and used as a loading control. For positive assay controls, deferoxamine-induced PC-3LN5 cell lysates (16 h treatment) were used for HIF-1α and LDH-A, deferoxamine-induced HCT116 human colon carcinoma cell lysates (16 h treatment) for c-Myc, and normal mouse brain for GLUT-1. Following c-Myc and LDH-A determination, immunoblots were stripped using re-blot stripping buffer (Millipore) and reprobed with anti-β-actin antibody as described above. Anti-mouse (1 : 5000), anti-rabbit (1 : 2000) and anti-goat (1 : 10 000) horseradish peroxidise-conjugated secondary antibodies were used, with subsequent detection using the chemiluminescent substrate ECL + (all GE Healthcare).

GLUT-1 immunocytofluorescence

PC-3LN5 cells were seeded in six-well plates (Corning Incorporated) using 20 × 20 mm^2 coverslips and allowed to adhere overnight. The following day, the medium was replaced with either fresh or NSC-134754 supplemented medium for 30 min before exposure to hypoxic (1% O_2) conditions. After incubation, the cells were rinsed in PBS and fixed with ice-cold methanol for 5 min. Non-specific binding was blocked with 5% donkey serum (Sigma-Aldrich, Poole, UK) followed by incubation for 90 min with goat anti-human GLUT-1 (Santa Cruz Biotechnology, 1 : 100). After several washes, cells were incubated for 1 h, protected from light, with Dylight549-conjugated donkey anti-goat antibody (Jackson Immunoresearch, West Grove, PA, USA, 1 : 200). Nuclei were counterstained with DAPI (Sigma-Aldrich), mounted with vectashield (Vector Laboratories, Peterborough, UK) and imaged with a BX51 microscope (Olympus Optical, London, UK) interfaced to a PC running by CellP (Soft Imaging System, Münster, Germany).

MRS of cell extracts and media

Semi-confluent PC-3LN5 cells plated in T75 cm^2 flasks (Corning Incorporated) were treated with 7.5 μM NSC-134754 (5 × GI$_{50}$), and subsequently harvested following 24 h in hypoxia (1% O_2). Cells were washed with ice-cold PBS and fixed with ice-cold methanol. After 10 min, adherent cells were removed by mechanical scraping and metabolites were extracted from cells using a dual-phase extraction method (Tyagi et al, 1996). Samples were freeze-dried, resuspended in D_2O and analysed using ^{1}H-MRS. Conditioned cell culture medium was also collected and analysed by ^{1}H-MRS. The internal standard sodium 3-trimethylsilyl-2,2,3,3-tetradeuteropropionate (TSP) was added to the samples for chemical shift calibration and quantification. ^{1}H-MR spectra were acquired on a 500-MHz Bruker spectrometer (Ettlingen, Germany). A pulse and acquire with water suppression MR sequence was used (pulse angle of 45°, repetition time of 3 s, 256 averages (64 averages for media samples), spectral width of 7500 Hz). Metabolite concentrations were determined through the summation of all resonance integrals to which each metabolite contributes, using the Bruker Topspin-2 NMR software package, normalised relative to the peak integral of the internal reference TSP and cell number.

Propagation of tumour xenografts

All experiments were performed in accordance with the local ethical review panel, the UK Home Office Animals (Scientific Procedures) Act 1986, and the United Kingdom Co-ordinating Committee on Cancer Research guidelines (Workman et al, 2010). Male NCr nude mice were injected orthotopically with 1×10^5 PC-3LN5 cells in 50 μl serum-free medium into the ventral prostate gland. Tumours were selected for imaging when they reached a volume of ~ 1 cm in diameter (assessed by palpation).

Magnetic resonance imaging

Mice were administered with 100 mg kg^{-1} NSC-134754 i.p. or left untreated, and imaged either 6, 24 or 48 h later. Magnetic resonance imaging was performed on a 7-T horizontal bore Bruker microimaging system using a 3-cm birdcage coil. Anaesthesia was induced by intraperitoneal injection of fentanyl citrate (0.315 mg ml^{-1}) plus fluanisone (10 mg ml^{-1} (Hypnorm; Janssen Pharmaceutical Ltd., High Wycombe, UK)), midazolam (5 mg ml^{-1} (Hypnovel; Roche)), and water (1:1:2). A lateral tail vein was cannulated with a 27-G butterfly catheter (Hospira, Royal Leamington Spa, Warwickshire, UK) for remote administration of the contrast agent Gd-DTPA (Magnevist, Schering, Berlin, Germany). Mice were positioned supine in the coil, and their core temperature was maintained at 37 $^{\circ}$C with warm air blown through the magnet bore. Multi-slice T_2-weighted contiguous 1-mm thick axial images were first acquired for localisation of the tumour and subsequent quantitation of tumour volume. A diffusion-weighted (DW) spin-echo sequence ($T_R = 1500$ ms, b-value = 150–750 s mm^{-2}, 4 b-values, 1 average) was then used to determine the tumour apparent diffusion coefficient (ADC) from a single 1-mm thick axial slice through the centre of the tumour. Dynamic contrast-enhanced MRI data were then acquired from the same slice using an inversion recovery (IR) trueFISP sequence with one baseline scan ($T_I = 130$–2592 ms, 20 inversion times, $T_R = 4$ ms, $T_E = 2$ ms, 12 averages) and 75 dynamic scans ($T_I = 130$–1037 ms, 8 inversion times, $T_R = 4$ ms, $T_E = 2$ ms, temporal resolution = 9 s, 2 averages) before and following i.v. injection of 0.1 mmol kg^{-1} Gd-DTPA (Boult et al, 2011). Immediately following MRI, the hypoxia marker pimonidazole (60 mg kg^{-1}; Hypoxyprobe Inc., Burlington, VT, USA) was administered intraperitoneally (Raleigh et al, 1999). After 45 min, Hoechst 33342 (15 mg kg^{-1}; Sigma-Aldrich), a marker for perfused vessels (Smith et al, 1988), was injected via a lateral tail vein. After 1 min tumours were rapidly excised, and cut threeways; two-thirds were snap frozen over liquid nitrogen for subsequent fluorescence microscopy and VEGF analysis, respectively, while the remaining third was fixed in 10% formal saline (v/v) for embedding in paraffin.

Magnetic resonance imaging data analysis

Diffusion-weighted and DCE-MRI data were fitted on a pixel-by-pixel basis using in-house software (ImageView, developed in IDL, ITT Visual Information Systems, Boulder, CO, USA). Diffusion data were fitted using a Bayesian maximum a posteriori approach that took into account the Rician distribution of noise in magnitude MR data and provided estimates of the ADC, allowing the median ADC value in each tumour to be calculated (Walker-Samuel et al, 2009). Inversion recovery trueFISP data were fitted using a similar approach, but which also utilised the dual-relaxation sensitivity (T_1 and T_2) of the IR-trueFISP sequence and incorporated the Tofts and Kermode pharmacokinetic model (Boult et al, 2011). This provided estimates of K^{trans}, dependent on permeability, blood flow and blood volume. T_2-weighted images were segmented using hand-drawn regions of interest (ROIs) to allow quantitation of tumour volumes to be calculated.

Immunofluorescence/histochemical analysis

For immunofluorescence, serial 10 μm frozen tissue sections were cut, and slides fixed in ice-cold acetone for 10 min before being imaged on a fluorescence microscope for Hoechst 33342 uptake. Fluorescence signals from tumour sections were then recorded at 365 nm using a motorised scanning stage (Prior Scientific Instruments, Cambridge, UK) attached to a BX51 microscope driven by image analysis software (CellP). Immediately following Hoechst 33342 image acquisition, the slides were blocked with 2% bovine serum albumin (w/v) (Vector) and 5% goat serum albumin (v/v) (Sigma-Aldrich) in PBS for 30 min, followed by incubation for 2 h with a FITC-conjugated mouse anti-pimonidazole antibody protected from light (Hypoxyprobe Inc., 1:500). The slides were then washed and imaged at 450–490 nm. All slides were then stained with haematoxylin and eosin (H&E), dehydrated through a series of alcohols and xylene, coverslipped and imaged under bright field illumination.

Paraffin-embedded tissue was cut into 5 μm sections, dewaxed and rehydrated through xylene and graded alcohols. Antigen retrieval was performed using the microwave heat-induced method with 10 mM citrate buffer (pH 6.0) for 20 min (Shi et al, 1991). Slides were then blocked for 1 h with serum-free protein block (Dako, Ely, UK), incubated overnight with either rabbit anti-human HIF-1α (Abcam, Cambridge, UK, 1:100) or rabbit anti-human GLUT-1 (Millipore, 1:100). The following day, slides were washed twice and incubated for 15 min with peroxidase block (Dako) to quench endogenous peroxidase activity. After further washes, an anti-rabbit HRP polymer (Dako) was applied to slides and after a 40-min incubation, staining was visualised using 3,3-diaminobenzidine + (Dako). Sections were counterstained with Mayer's haematoxylin, dehydrated through graded alcohols and mounted.

Image analysis software (CellP) was used for all image post-processing. For perfused vessels (Hoechst 33342), tumour hypoxia (pimonidazole) and necrosis (H&E), two/three sections per tumour from a minimum of four tumours from each treatment group were analysed. Regions of interest for each tumour section were defined and an intensity threshold level set per tumour to account for variation in staining. Fluorescence particles were detected and expressed as a mean percentage of each tumour section. For the quantitation of Hoechst 33342 perfused area and pimonidazole adducts, the H&E composite image was used to exclude any residual glandular prostate tissue and necrosis from analysis. For GLUT-1 and HIF-1α analysis, 12 fields of view from a minimum of four tumours from each group were assessed and scored using a semi-quantitative method. Glucose transporter-1 membrane staining was scored as follows: 0 = absence of staining, 1 = <10% staining, 2 = <50% staining, 3 = >50% staining (Mayer et al, 2004). For HIF-1α analysis, positive expression was defined by nuclear staining and scored as follows: 0 = absence of staining, 1 = <25% staining, 2 = 25–50% staining, 3 = 50–75% staining, 4 = >75% staining.

VEGF protein analysis

A minimum of four tumours from control, 6 and 24 h treatment groups were analysed. Snap frozen tumours were ground using a bead grinder homogeniser (Precellys, Stretton Scientific, Derbyshire, UK) in freshly prepared lysis buffer. Samples were subsequently assessed for total protein concentration using the Bradford method according to the manufacturer's instructions (Pierce Protein Research Products, Thermo Fisher Scientific, Cramlington, UK) and human VEGF concentration per mg of total protein was determined by ELISA (R&D Systems, Abingdon, UK), according to the manufacturer's protocol.

Statistical analysis

Statistical significance was defined as a P-value <0.05. Two-tailed Student's t-test, one-way ANOVA or Kruskal–Wallis with Bonferroni correction were used where appropriate.

RESULTS

NSC-134754 reduces hypoxia-induced HIF-1α protein expression and the target gene GLUT-1 *in vitro*

The SRB assay was used to determine any anti-proliferative effects of NSC-134754 on PC-3LN5 cells *in vitro*. A GI$_{50}$ value of $\approx 1.5 \mu mol\,l^{-1}$ after treatment for 72 h in hypoxia (1% O$_2$) was established. To determine whether the anti-proliferative effect of NSC-134754 was related to HIF-1α protein levels, western blot analysis of 1×, 3× and 5× GI$_{50}$ were performed on PC-3LN5 cells incubated for 6 or 24 h in hypoxia. NSC-134754 reduced HIF-1α protein expression in a dose-dependent manner, with complete inhibition seen at 6 h and decreased expression at 24 h with 5× GI$_{50}$ (Figure 1A). The effect of NSC-134754 on GLUT-1, a major downstream target of HIF-1 and a membrane-bound protein involved in intracellular glucose transport, was also examined. Western blot analysis demonstrated a reduction in GLUT-1 expression (3× and 5× GI$_{50}$) after 6 and 24 h in hypoxia (Figure 1B). Immunocytofluorescence confirmed control cells exposed to hypoxic conditions for 6 and 24 h exhibited strong GLUT-1 membranous staining with diffuse cytoplasmic staining,
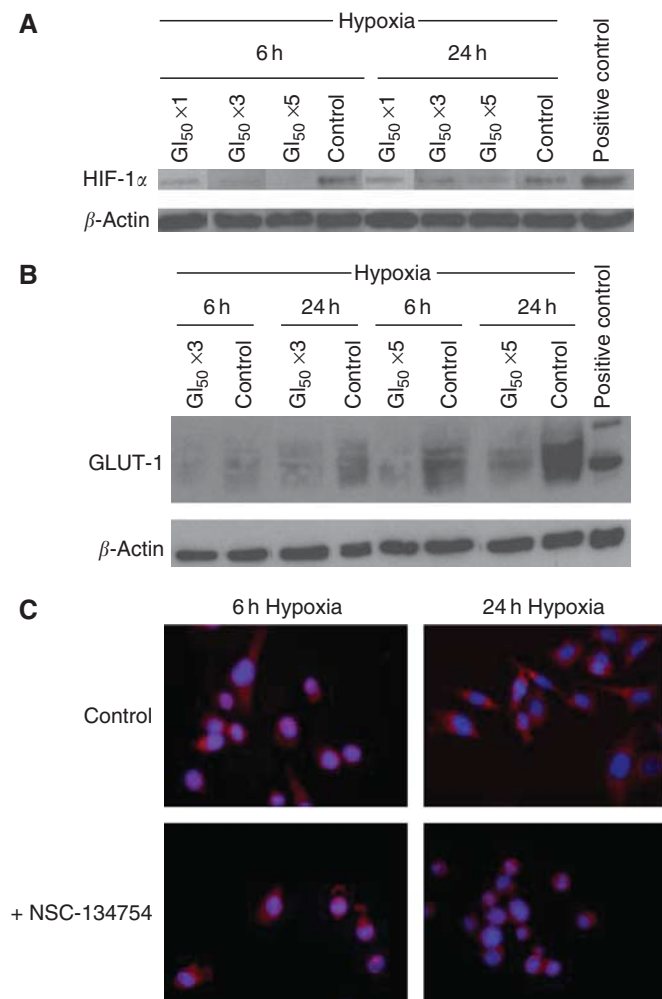
which was particularly evident at 24 h. In cells treated with NSC-134754 (5× GI$_{50}$) for 6 or 24 h in hypoxia, an overall decrease in GLUT-1 staining compared with control cells was apparent (Figure 1C). The DAPI-stained nuclei were morphologically similar between control and treated cells, with negligible chromatin condensation and/or nuclear fragmentation (Figure 1C).

NSC-134754 alters cellular metabolism and downregulates LDH-A and c-Myc protein expression *in vitro*

High-resolution ^{1}H-MRS was used to assess the biochemical effects of decreased GLUT-1 expression with NSC-134754 *in vitro*. Aqueous extracts of cells and conditioned media treated with NSC-134754 (5× GI$_{50}$) and exposed to 24 h hypoxia (1% O$_2$) were analysed. Representative ^{1}H-MRS spectra of cell extracts with metabolic changes induced by NSC-134754 are shown in Figure 2A. Conditioned media from treated cells showed a statistically significant decrease in glucose consumption ($P < 0.05$) and lactate production ($P < 0.05$) compared with control cells (also incubated in hypoxia). Intracellular lactate concentration was not significantly different between groups (Figure 2C). However, treatment with NSC-134754 significantly increased intracellular glucose by >4-fold compared with controls ($P < 0.01$) (Figure 2B and C). Other metabolites of note were (i) glutamine and glutamate, both of which were significantly increased in uptake from conditioned media and had significantly increased intracellular levels in NSC-134754-treated cells compared with controls ($P < 0.05$) and (ii) intracellular choline metabolites, of which a highly significant ($P < 0.01$) increase in glycerophosphocholine and significant ($P < 0.05$) decrease in phosphocholine was determined in the treated cells (data not shown). The effect of NSC-134754 on LDH-A, a HIF-regulated enzyme involved in the conversion of pyruvate to lactate, was also determined (Dang and Semenza, 1999). In addition c-Myc, a proto-oncogene previously reported to stimulate mitochondrial metabolism, was assessed (Wise *et al*, 2008). Western blot analysis demonstrated both a reduction in LDH-A expression and c-Myc expression (5× GI$_{50}$) after 6 and 24 h in hypoxia compared with untreated control (Figure 2D).

NSC-134754 increases tumour water diffusion at 24 h followed by tumour necrosis at 48 h

We next investigated the acute effects of a single i.p. dose of $100\,mg\,kg^{-1}$ NSC-134754 *in vivo* using DW-MRI. There was no significant difference in mean tumour volume between the treatment groups or the control group ($P > 0.1$). Representative ADC maps calculated for control and treated mice are shown in Figure 3A. Median ADC values for individual tumours are shown in Figure 3B. Tumour ADC was significantly higher 24 and 48 h post-treatment with NSC-134754 ($P < 0.05$ and $P < 0.01$, respectively) compared with control and 6 h post-treatment groups. Morphological assessment using H&E demonstrated a central core of necrosis as a general feature of PC-3LN5 tumours at the time of treatment/imaging (Figure 3C). Quantitative analysis revealed an associated increase in necrosis 24 h after administration with NSC-134754 ($P = 0.17$), with a statistically significant increase at 48 h post-treatment ($P < 0.05$) compared with control (Figure 3D).

NSC-134754 induces a transient decrease in HIF-1α followed by a sustained decrease in GLUT-1

The translational effects of a single i.p. dose of $100\,mg\,kg^{-1}$ NSC-134754 on the HIF pathway in PC-3LN5 orthotopic prostate tumours were assessed. Cytoplasmic expression of HIF-1α was present throughout all tumours, while nuclear staining was particularly evident in peri-necrotic zones (Figure 4A). Nuclear HIF-1α was temporally and significantly lower in treated tumours
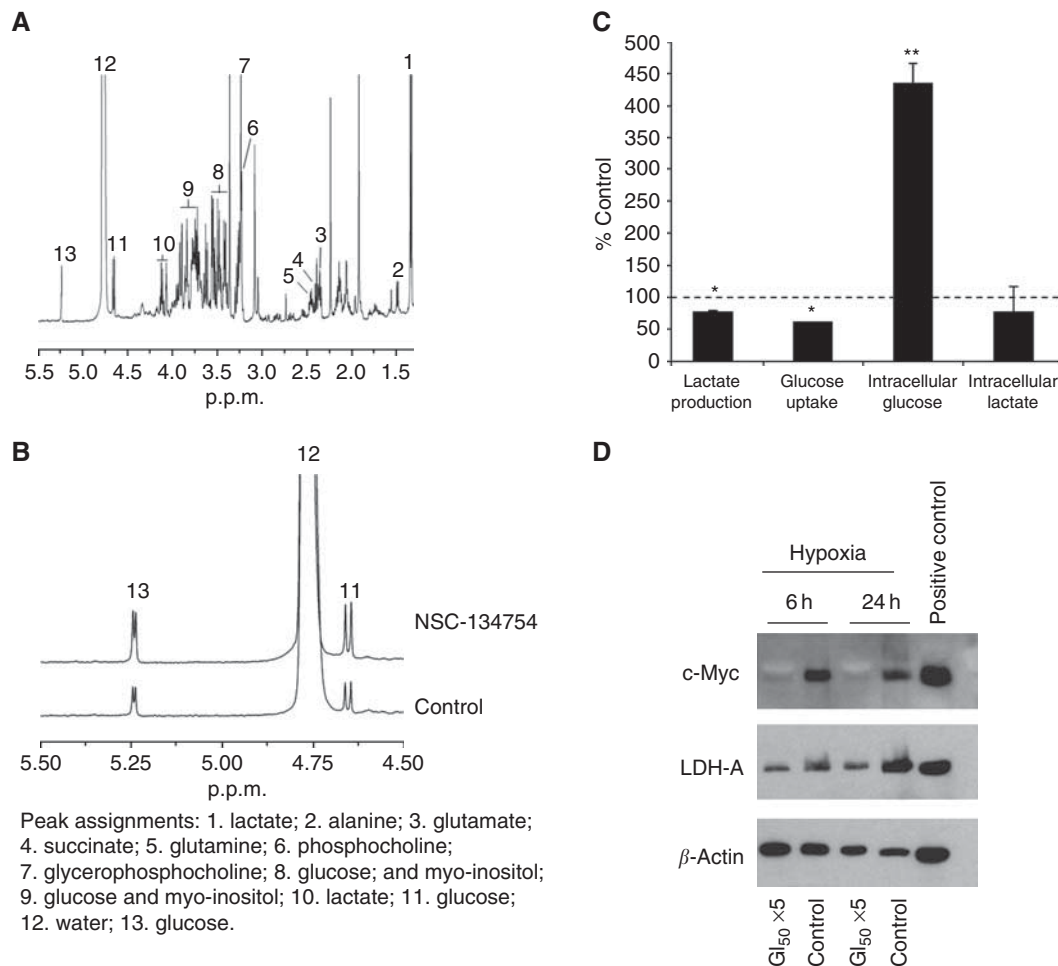

Figure 1 Molecular effects of NSC-134754 on the HIF pathway in PC-3LN5 cells *in vitro* exposed to hypoxia (1% O$_2$) for 6 or 24 h. Representative western blots showing (**A**) HIF-1α expression (1×, 3× and 5× GI$_{50}$) and (**B**) GLUT-1 expression (3× and 5× GI$_{50}$). (**C**) Immunocytofluorescence expression of GLUT-1 (5× GI$_{50}$). For internal positive control, lysates from cells incubated for 16 h with the hypoxia mimetic deferoxamine (HIF-1α) and normal murine brain tissue (GLUT-1) were used.

Figure 2 PC-3LN5 cells were incubated in hypoxia (1% O_2) for 24 h ± 5 × GI$_{50}$ NSC-134754. (**A**) Representative ^{1}H-MRS spectrum of a cell extract from cells treated with NSC-134754. (**B**) ^{1}H-MRS spectra of cell extracts expanded in the region of 4.5–5.5 p.p.m., clearly illustrating the effect of NSC-134754 on glucose resonances compared with untreated control. (**C**) Concentration ratios of glucose metabolites in PC-3LN5 cells and conditioned media following treatment with NSC-134754, expressed as a percentage of untreated control. Results are expressed as mean percentage of control ± 1 s.e.m., *$P < 0.05$, **$P < 0.01$, $n \geqslant 3$. (**D**) Western blots showing the effects of NSC-134754 on c-Myc and LDH-A protein expression after 6 and 24 h treatment in hypoxia compared with untreated control.

at 6 h compared with control ($P < 0.05$). After 24 h, HIF-1α staining between the groups was comparable (Figure 4B). The HIF-1 target gene, GLUT-1, demonstrated similar patterns of membranous expression in the 6, 24 and 48 h post-treatment tumours. In contrast, control tumours exhibited strong, diffuse GLUT-1 expression throughout (Figure 4A). Glucose transporter-1 expression was significantly lower in treated tumours at 24 h compared with control ($P < 0.01$), and continued to be downregulated for at least 48 h ($P < 0.01$) (Figure 4B). No significant difference in tumour VEGF, assayed by ELISA, was found between the treatment groups (Figure 4B).

NSC-134754 is associated with a transient increase in tumour hypoxia that precedes an increase in tumour necrosis, and is independent of changes in vessel perfusion

Given the intrinsic role of the HIF pathway in cellular adaptation to hypoxia, we also investigated the vascular and oxygenation status of tumours. Dynamic contrast-enhanced MRI was used to estimate K^{trans}, a compound imaging biomarker of both vascular permeability and blood flow (Leach *et al*, 2005). No significant difference in K^{trans} was determined at either 6 or 24 h following treatment with NSC-134754 compared with controls (data not shown). *Ex-vivo* composite images of hypoxia and perfusion for

representative tumours from control, 6, 24 and 48 h treated mice are shown in Figure 5A. Tumour hypoxia was determined with pimonidazole staining, a 2-nitroimidazole that forms bioreductive adducts at typically < 10 mm Hg (Raleigh *et al*, 1999). After 6 h of treatment with NSC-134754, mean percentage pimonidazole adduct formation was not significantly different in treated *vs* control groups. At 24 h, the mean percentage pimonidazole adduct area was significantly greater in treated mice compared with controls ($P < 0.05$). At 48 h post-treatment, no statistical significance in mean percentage pimonidazole adduct formation compared with controls was observed (Figure 5B). Vessel perfusion, measured using Hoechst 33342, did not significantly differ between control, 6, 24 and 48 h treated tumours (Figure 5B).

DISCUSSION

Tumour hypoxia represents a major obstacle to the treatment success of radiotherapy and certain types of chemotherapy (Tatum *et al*, 2006). In response to hypoxia, HIF-1 activates the transcription of genes whose protein products are involved in cell survival, angiogenesis, glycolytic metabolism and cell invasion/metastasis (Semenza, 2003). Small-molecule inhibitors that target components of the HIF pathway are thus being pursued as an anticancer strategy. In the present study, we have investigated the
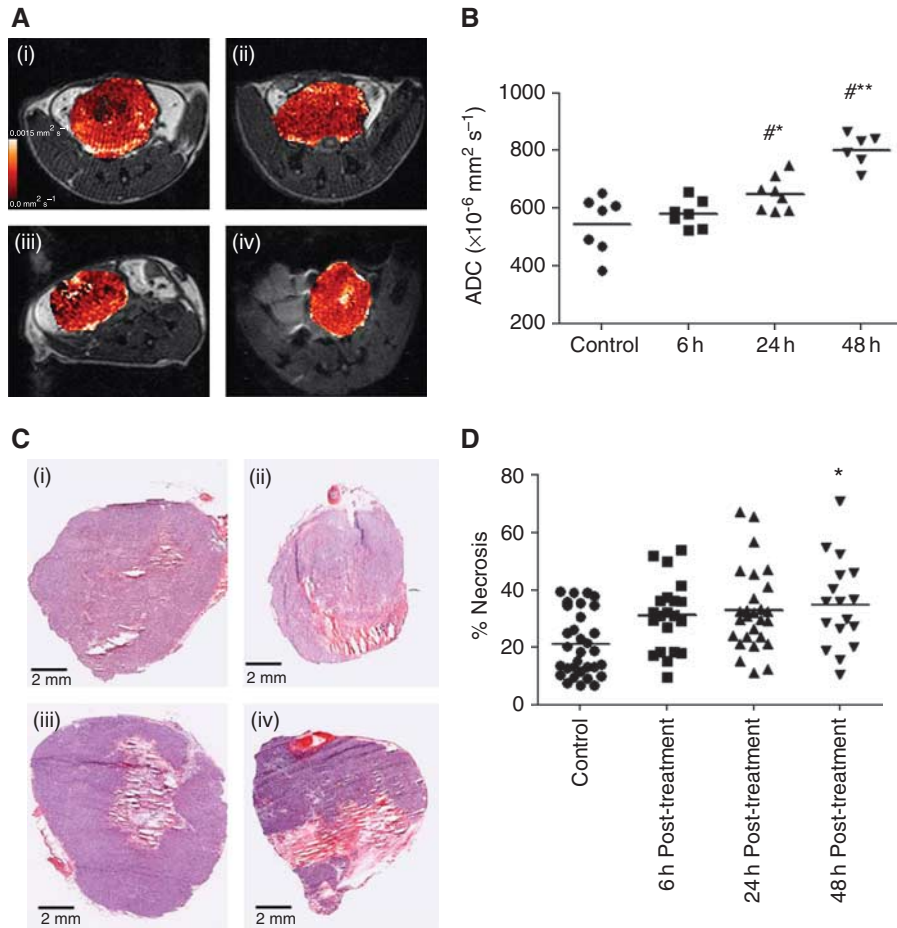
Figure 3 MRI determination of tumour water diffusivity (ADC) and *ex-vivo* histological assessment of necrosis with 100 mg kg^{-1} NSC-134754 at 6, 24 or 48 h post-treatment compared with untreated controls. Each time point represents a separate cohort of animals. (**A**) Representative DW images overlaid with ADC maps from mice bearing PC-3LN5 orthotopic prostate tumours (i) control (ii) 6 h post-treatment (iii) 24 h post-treatment and (iv) 48 h post-treatment. (**B**) Scatter plot of individual tumour median ADC values. Mean group values are indicated by the horizontal bar. (**C**) H&E composite images of orthotopic PC-3LN5 prostate tumours (i) control (ii) 6 h post-treatment, (iii) 24 h post-treatment and (iv) 48 h post-treatment. (**D**) Scatter plot of individual tumour necrosis scores (%). $^{\#}P < 0.05$ compared with 6 h treatment, $*P < 0.05$, $**P < 0.01$ compared with control, $n \geqslant 6$.

acute effects of the small-molecule HIF-pathway inhibitor NSC-134754 on human prostate cancer cells *in vitro* and murine orthotopic prostate tumours *in vivo*. Previous studies have demonstrated that HIF inhibition results in metabolic reprogramming, with an attenuation of anaerobic glycolysis and an increase in mitochondrial metabolism (Cairns *et al*, 2007). Here, we have shown that treatment with NSC-134754 alters the metabolic profile of PC-3LN5 cells, downregulating GLUT-1 and LDH-A, resulting in an overall reduction in glucose consumption and lactate production. These findings are in agreement with the metabolic response to pharmacological HIF inhibition reported by others (Jordan *et al*, 2005a; Moeller *et al*, 2005). We also show that this NSC-134754-induced downregulation in glycolytic metabolism was accompanied by an increase in glutamine/glutamate metabolism. Cellular uptake of glutamine can be used for protein synthesis, but is primarily converted to glutamate, which is further catabolised to α-ketoglutarate for further oxidation in the tricarboxylic acid (TCA) cycle. Recent studies have suggested that the proto-oncogene c-Myc is a major mediator in stimulating mitochondrial glutaminolysis (Wise *et al*, 2008). Furthermore, an associative relationship between HIF-1 and c-Myc has also been demonstrated, whereby c-Myc and HIF-1 co-operate to accelerate both glycolysis and angiogenesis (Kim *et al*, 2007). We thus sought to determine whether the effect of HIF inhibition (and associated metabolic changes) influenced c-Myc protein expression. PC-3LN5

cells strongly expressed c-Myc protein under conditions of hypoxia. Interestingly, treatment with NSC-134754 induced almost complete suppression of c-Myc protein expression. Taken together, NSC-134754 appears to exhibit dual-activity against both the HIF pathway and c-Myc. Further studies will be required in order to determine the mechanism of HIF/c-Myc protein repression, particularly to address whether these effects are synergistic or independently produced.

Many glycolytic enzymes are known to be gene targets of HIF-1 (Semenza, 2003). Thus, a reduction in the availability of, for example, hexokinase 1/2 and/or glyceraldehyde 3-phosphate dehydrogenase, could conceivably lead to a downregulation in glycolysis and subsequent increase in glucose. We observed a significant increase in intracellular glucose following treatment with NSC-134754. To our knowledge, increased intracellular glucose with a small-molecule inhibitor of the HIF pathway is a novel finding. Increased intracellular glucose, coupled with decreased glucose uptake, has been reported with the tyrosine kinase inhibitor imatinib (Klawitter *et al*, 2009). Notably, imatinib has also been shown to (indirectly) downregulate HIF-1 (Litz and Krystal, 2006). In contrast, maintenance of basal intracellular glucose has been shown to act as an anti-apoptotic survival mechanism (Weihua *et al*, 2008). Following treatment with NSC-134754, our observations were of a reduction in cellular proliferation, with no associated evidence of nuclear morphology
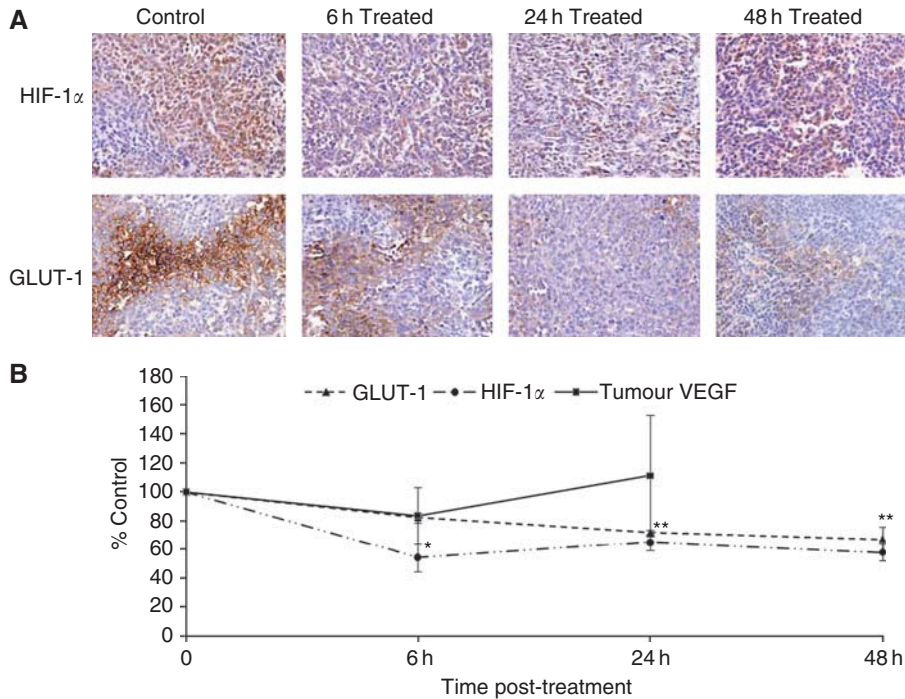
Figure 4 Targeted and transcriptional effects of NSC-134754 on PC-3LN5 murine orthotopic prostate tumours at 6, 24 and 48 h after treatment compared with untreated control. (**A**) Representative images of HIF-1α and GLUT-1 expression. (**B**) Summary of mean differences in expression of tumour HIF-1α, GLUT-1 and VEGF in NSC-134754-treated groups compared with control: ● HIF-1α, ▲ GLUT-1, ■ VEGF. Values are represented as mean ± 1 s.e.m. *$P<0.05$, **$P<0.01$ compared with control.
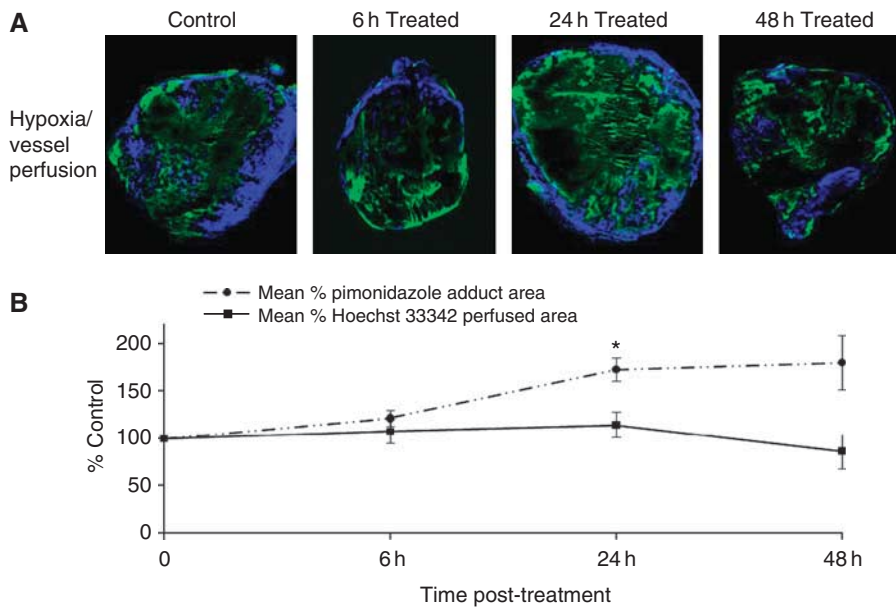

Figure 5 Microenvironmental effects of NSC-134754 on murine orthotopic PC-3LN5 prostate tumours at 6, 24 and 48 h after treatment compared with untreated controls. (**A**) Representative composite fluorescence images demonstrating vessel perfusion (Hoechst 33342, blue) and hypoxia (pimonidazole adducts, green). (**B**) Summary of the quantitative analysis of tumour perfusion and hypoxia over time. Values are represented as mean ± 1 s.e.m., *$P<0.05$ compared with control.

characteristics of cellular death. Further studies will be required to elucidate the functional relevance of this finding, particularly with respect to therapeutic response. The impact of increased intracellular glucose on modalities based on the imaging of analogues of glucose (e.g., ^{18}F fluorodeoxyglucose positron emission tomography) will also be of relevance.

A number of alterations in metabolites known to be involved in lipid synthesis and turnover were also observed following

treatment with NSC-134754. These included a significant reduction in phosphocholine and highly significant increase in glycerophosphocholine. High levels of phosphocholine have been associated with increased membrane synthesis, a feature associated with rapidly dividing cancer cells (Moreno and Arús, 1996). Conversely, decreased phosphocholine accompanied with increased glycerophosphocholine has been reported with several molecularly targeted therapies (Beloueche-Babari et al, 2010). Overall, the

alterations in lipid metabolites induced with treatment suggest additional anti-cancer activity associated with NSC-134754 *in vitro*.

We sought to determine whether the metabolic changes and anti-proliferative effects of NSC-134754 observed *in vitro* would translate to anti-tumour effects *in vivo*. Typically, tumour ADC (measured using non-invasive MRI) is increased following successful anti-cancer therapy, and is associated with a loss in membrane integrity, an early feature of cellular death (before measurable changes in tumour volume) (Zhao *et al*, 1996; Chenevert *et al*, 2000; Padhani *et al*, 2009). Increased ADC has also been reported as an early response to the pharmacological HIF-1α inhibitor PX-478, presumably due to an increase in tumour necrosis (Jordan *et al*, 2005b). We have demonstrated that tumour ADC was significantly greater 24 and 48 h post-treatment with NSC-134754 compared with control. Importantly, the elevated ADC determined 24 h post-treatment preceded any histologically determined significant increase in tumour necrosis, which was reached 48 h post-treatment. This early, anti-tumourigenic response to NSC-134754 is also comparable with the time course of ADC changes reported pre-clinically with PX-478 (Jordan *et al*, 2005b). The mechanism(s) underlying decreased tumour cellularity with HIF inhibition are not yet understood, and given the pleiotropic effects that HIF inhibition likely elicits, will require extensive investigation. Nevertheless, DW-MRI appears to provide a non-invasive imaging approach in which to detect acute response to HIF inhibition.

Dynamic contrast-enhanced MRI has previously been shown to detect early effects of HIF inhibition on tumour vessel physiology and vascular flow (Jordan *et al*, 2005b). Using DCE-MRI, we were unable to demonstrate any anti-angiogenic or inhibitory effects on vessel perfusion with NSC-134754. This surprising finding may be attributed to differences in dose/response timings and/or the type of MR-contrast agent used. For example, we utilised the clinically approved low molecular weight gadolinium contrast agent Magnevist, sensitive to changes in both vascular permeability and perfusion, whereas others have used a macromolecular contrast agent providing greater sensitivity to alterations in vascular permeability alone (Jordan *et al*, 2005b). *Ex-vivo* techniques to measure vessel perfusion and tumour VEGF were also in agreement with our DCE-MRI findings, with no anti-angiogenic response induced with NSC-134754. It should be noted that HIF-independent pathways may contribute to angiogenesis when the HIF pathway is blocked. For example, the resultant accumulation of hydrogen peroxide increases NF-κB, resulting in the upregulation of the pro-angiogenic factors angiopoietin-2 and VEGF (Mizukami *et al*, 2007). Thus other mechanisms, aside from HIF, may regulate tumour vascularity in the PC-3LN5 model. Importantly, and despite an absence of change in vascular perfusion, an increase in tumour hypoxia was detected 24 h post-treatment with NSC-134754. Although HIF inhibition has been shown to increase tumour hypoxia due to changes in blood flow, perfusion and tumour VEGF concentrations (Harada *et al*, 2009), targeting HIF-1 (or components of the HIF pathway) has also been shown to increase mitochondrial metabolism, which in turn increases the rate of oxygen consumption (Cairns *et al*, 2007). Increased mitochondrial metabolism in malignant cells increases the generation of reactive oxygen species, which are linked to cellular death (Le *et al*, 2010). The increase in tumour hypoxia with NSC-134754, independent of changes in vascular function, suggests that the anti-tumour activity of this agent may be primarily metabolically driven. Thus, NSC-134754 may increase tumour hypoxia via utilisation of a non-glycolytic energy source, exhausting available oxygen through the TCA cycle, and ultimately leading to an increase in tumour necrosis. Interestingly, though acute vascular effects were reported with the HIF-1α inhibitor PX-478, these appeared to be superceded by metabolic changes, suggesting that the overall therapeutic effect of HIF inhibition with PX-478 was also metabolically derived (Welsh *et al*, 2004). Collectively, these data suggest that the evaluation of novel HIF inhibitors will benefit from both ^{1}H-MRS and MRI investigations.

Finally, increased expression of HIF-1α and the downstream target GLUT-1 have been associated clinically with tumour metastasis and poor prognosis (Younes *et al*, 1997; Haber *et al*, 1998; Zhong *et al*, 1999). We have confirmed that NSC-134754 exhibits both targeted and translational effects *in vivo* via *ex vivo* detection of HIF-1α and GLUT-1. Using immunohistochemistry, we have demonstrated that a single i.p. dose of NSC-134754 decreases HIF-1α expression for at least 6 h. Furthermore, the temporal increase in tumour hypoxia induced in treated tumours at 24 h was not accompanied by a subsequent increase in HIF-1α expression compared with controls. This may indicate that NSC-134754 maintains a dampened hypoxia-induced HIF response in the PC-3LN5 model for at least 24 h after administration. Membrane expression of the downstream target GLUT-1 was decreased 24 h post-NSC-134754. Interestingly, this decrease was sustained out to 48 h, providing further evidence of the potent metabolic effects of this agent. A similar temporal response in GLUT-1 expression has also been reported with PX-478 (Welsh *et al*, 2004).

In conclusion, HIF-pathway inhibitors are an emerging class of therapeutics that offer great potential, but are also beginning to reveal the complexity underlying tumour growth and survival in the hypoxic microenvironment. The cascade of gene transcription downstream of HIF-1 impacts on angiogenic, metabolic, proliferative and metastatic pathways, thus HIF-pathway inhibitors in turn may exhibit a wide range of effects. The results reported here demonstrate that the small-molecule HIF-pathway inhibitor NSC-134754 induces metabolic reprogramming *in vitro*, and acute functional changes independent of vascular effects *in vivo*. Importantly, the early, anti-tumour effects of NSC-134754 were observed non-invasively with DW-MRI. Quantitation of tumour ADC thus appears to be an attractive, clinically translatable imaging biomarker sensitive to therapeutic response to HIF-pathway inhibition. Further investigation into the action of NSC-134754 will be required in order to determine the utility of this compound, either as a single agent or in combination. In particular, the timing of the microenvironmental effects of NSC-134754 and those of other potential HIF inhibitors will be an important factor to consider when combining these types of agents with treatment regimens that are reliant on tumour oxygenation levels, for example, radiotherapy.

REFERENCES

Bardos JI, Ashcroft M (2004) Hypoxia-inducible factor-1 and oncogenic signalling. *Bioessays* **26**(3): 262–269

Beloueche-Babari M, Chung YL, Al-Saffar NM, Falck-Miniotis M Leach MO (2010) Metabolic assessment of the action of targeted cancer

Translational Therapeutics

therapeutics using magnetic resonance spectroscopy. *Br J Cancer* **102**(1): 1–7

Boult JK, Walker-Samuel S, Jamin Y, Leiper JM, Whitley GS, Robinson SP (2011) Active site mutant dimethylarginine dimethylaminohydrolase 1 expression confers an intermediate tumour phenotype in C6 gliomas *J Pathol* **225**(3): 344–352

Cairns RA, Papandreou I, Sutphin PD, Denko NC (2007) Metabolic targeting of hypoxia and HIF1 in solid tumors can enhance cytotoxic chemotherapy. *Proc Natl Acad Sci USA* **104**(22): 9445–9450

Carmeliet P, Dor Y, Herbert JM, Fukumura D, Brusselmans K Dewerchin M, Neeman M, Bono F, Abramovitch R, Maxwell P, Koch CJ, Ratcliffe P, Moons L, Jain RK, Collen D, Keshert E (1998) Role of HIF-1alpha in hypoxia-mediated apoptosis, cell proliferation and tumour angiogenesis. *Nature* **394**(6692): 485–490

Chau NM, Rogers P, Aherne W, Carroll V, Collins I, McDonald E, Workman P, Ashcroft M (2005) Identification of novel small molecule inhibitors of hypoxia-inducible factor-1 that differentially block hypoxia-inducible factor-1 activity and hypoxia-inducible factor-1alpha induction in response to hypoxic stress and growth factors. *Cancer Res* **65**(11): 4918–4928

Chenevert T, Stegman L, Taylor J, Robertson P, Greenberg H, Rehemtulla A, Ross B (2000) Diffusion magnetic resonance imaging: an early surrogate marker of therapeutic efficacy in brain tumors. *J Natl Cancer Inst* **92**(24): 2029–2036

Dang CV, Semenza GL (1999) Oncogenic alterations of metabolism. *Trends Biochem Sci* **24**(2): 68–72

Gray LH, Conger AD, Ebert M, Hornsey S, Scott OC (1953) The concentration of oxygen dissolved in tissues at the time of irradiation as a factor in radiotherapy. *Br J Radiol* **26**(312): 638–648

Griffiths JR, McSheehy PM, Robinson SP, Troy H, Chung YL, Leek RD, Williams KJ, Stratford IJ, Harris AL, Stubbs M (2002) Metabolic changes detected by *in vivo* magnetic resonance studies of HEPA-1 wild-type tumors and tumors deficient in hypoxia-inducible factor-1beta (HIF-1beta): evidence of an anabolic role for the HIF-1 pathway. *Cancer Res* **62**(3): 688–695

Haber RS, Rathan A, Weiser KR, Pritsker A, Itzkowitz SH, Bodian C, Slater G, Weiss A, Burstein DE (1998) GLUT1 glucose transporter expression in colorectal carcinoma: a marker for poor prognosis. *Cancer* **83**(1): 34–40

Harada H, Itasaka S, Zhu Y, Zeng L, Xie X, Morinibu A, Shinomiya K, Hiraoka M (2009) Treatment regimen determines whether an HIF-1 inhibitor enhances or inhibits the effect of radiation therapy. *Br J Cancer* **100**(5): 747–757

Jordan BF, Black K, Robey IF, Runquist M, Powis G, Gillies RJ (2005a) Metabolite changes in HT-29 xenograft tumors following HIF-1alpha inhibition with PX-478 as studied by MR spectroscopy *in vivo* and *ex vivo*. *NMR Biomed* **18**(7): 430–439

Jordan BF, Runquist M, Raghunand N, Baker A, Williams R, Kirkpatrick L, Powis G, Gillies RJ (2005b) Dynamic contrast-enhanced and diffusion MRI show rapid and dramatic changes in tumor microenvironment in response to inhibition of HIF-1alpha using PX-478. *Neoplasia* **7**(5): 475–485

Kim JW, Gao P, Liu YC, Semenza GL, Dang CV (2007) Hypoxia-inducible factor 1 and dysregulated c-Myc cooperatively induce vascular endothelial growth factor and metabolic switches hexokinase 2 and pyruvate dehydrogenase kinase 1. *Mol Cell Biol* **27**(21): 7381–7393

Kioi M, Vogel H, Schultz G, Hoffman RM, Harsh GR, Brown JM (2010) Inhibition of vasculogenesis, but not angiogenesis, prevents the recurrence of glioblastoma after irradiation in mice. *J Clin Invest* **120**(3): 694–705

Klawitter J, Anderson N, Christians U, Leibfritz D, Eckhardt S, Serkova N (2009) Time-dependent effects of imatinib in human leukaemia cells: a kinetic NMR-profiling study. *Br J Cancer* **100**(6): 923–931

Le A, Cooper CR, Gouw AM, Dinavahi R, Maitra A, Deck LM, Royer RE, Vander Jagt DL, Semenza GL, Dang CV (2010) Inhibition of lactate dehydrogenase A induces oxidative stress and inhibits tumor progression. *Proc Natl Acad Sci USA* **107**(5): 2037–2042

Leach MO, Brindle KM, Evelhoch JL, Griffiths JR, Horsman MR, Jackson A, Jayson G, Judson IR, Knopp MV, Maxwell RJ, McIntyre D, Padhani AR, Price P, Rathbone R, Rustin G, Tofts PS, Tozer GM, Vennart W, Waterton JC, Williams SR, Workman P (2005) The assessment of antiangiogenic and antivascular therapies in early-stage clinical trials using magnetic resonance imaging: issues and recommendations. *Br J Cancer* **92**(9): 1599–1610

Litz J, Krystal GW (2006) Imatinib inhibits c-Kit-induced hypoxia-inducible factor-1alpha activity and vascular endothelial growth

factor expression in small cell lung cancer cells. *Mol Cancer Ther* **5**(6): 1415–1422

Maxwell PH, Dachs GU, Gleadle JM, Nicholls LG, Harris AL, Stratford IJ, Hankinson O, Pugh CW, Ratcliffe PJ (1997) Hypoxia-inducible factor-1 modulates gene expression in solid tumors and influences both angiogenesis and tumor growth. *Proc Natl Acad Sci USA* **94**(15): 8104–8109

Mayer A, Wree A, Hockel M, Leo C, Pilch H, Vaupel P (2004) Lack of correlation between expression of HIF-1alpha protein and oxygenation status in identical tissue areas of squamous cell carcinomas of the uterine cervix. *Cancer Res* **64**(16): 5876–5881

Michaelis LC, Ratain MJ (2006) Measuring response in a post-RECIST world: from black and white to shades of grey. *Nat Rev Cancer* **6**(5): 409–414

Mizukami Y, Kohgo Y, Chung DC (2007) Hypoxia inducible factor-1 independent pathways in tumor angiogenesis. *Clin Cancer Res* **13**(19): 5670–5674

Moeller BJ, Dreher MR, Rabbani ZN, Schroeder T, Cao Y, Li CY, Dewhirst MW (2005) Pleiotropic effects of HIF-1 blockade on tumor radio-sensitivity. *Cancer Cell* **8**(2): 99–110

Moreno A, Arús C (1996) Quantitative and qualitative characterization of 1H NMR spectra of colon tumors, normal mucosa and their perchloric acid extracts: decreased levels of myo-inositol in tumours can be detected in intact biopsies. *NMR Biomed* **9**(1): 33–45

Onnis B, Rapisarda A, Melillo G (2009) Development of HIF-1 inhibitors for cancer therapy. *J Cell Mol Med* **13**(9A): 2780–2786

Padhani A, Liu G, Koh D, Chenevert T, Thoeny H, Takahara T, Dzik-Jurasz A, Ross B, Van Cauteren M, Collins D, Hammoud D, Rustin G, Taouli B, Choyke P (2009) Diffusion-weighted magnetic resonance imaging as a cancer biomarker: consensus and recommendations. *Neoplasia* **11**(2): 102–125

Pugh CW, Ratcliffe PJ (2003) Regulation of angiogenesis by hypoxia: role of the HIF system. *Nat Med* **9**(6): 677–684

Raleigh JA, Chou SC, Arteel GE, Horsman MR (1999) Comparisons among pimonidazole binding, oxygen electrode measurements, and radiation response in C3H mouse tumors. *Radiat Res* **151**(5): 580–589

Robey IF, Lien AD, Welsh SJ, Baggett BK, Gillies RJ (2005) Hypoxia-inducible factor-1alpha and the glycolytic phenotype in tumors. *Neoplasia* **7**(4): 324–330

Sanderson S, Valenti M, Gowan S, Patterson L, Ahmad Z, Workman P, Eccles SA (2006) Benzoquinone ansamycin heat shock protein 90 inhibitors modulate multiple functions required for tumor angiogenesis. *Mol Cancer Ther* **5**(3): 522–532

Semenza GL (2000) Hypoxia, clonal selection, and the role of HIF-1 in tumor progression. *Crit Rev Biochem Mol Biol* **35**(2): 71–103

Semenza GL (2003) Targeting HIF-1 for cancer therapy. *Nat Rev Cancer* **3**(10): 721–732

Semenza GL, Roth PH, Fang HM, Wang GL (1994) Transcriptional regulation of genes encoding glycolytic enzymes by hypoxia-inducible factor 1. *J Biol Chem* **269**(38): 23757–23763

Shi SR, Key ME, Kalra KL (1991) Antigen retrieval in formalin-fixed, paraffin-embedded tissues: an enhancement method for immunohisto-chemical staining based on microwave oven heating of tissue sections *J Histochem Cytochem* **39**(6): 741–748

Skehan P, Storeng R, Scudiero D, Monks A, McMahon J, Vistica D, Warren JT, Bokesch H, Kenney S, Boyd MR (1990) New colorimetric cytotoxicity assay for anticancer-drug screening. *J Natl Cancer Inst* **82**(13): 1107–1112

Smith K, Hill S, Begg A, Denekamp J (1988) Validation of the fluorescent dye Hoechst 33342 as a vascular space marker in tumours. *Br J Cancer* **57**(3): 247–253

Tatum JL, Kelloff GJ, Gillies RJ, Arbeit JM, Brown JM, Chao KS, Chapman JD, Eckelman WC, Fyles AW, Giaccia AJ, Hill RP, Koch CJ, Krishna MC, Krohn KA, Lewis JS, Mason RP, Melillo G, Padhani AR, Powis G, Rajendran JG, Reba R, Robinson SP, Semenza GL, Swartz HM, Vaupel P, Yang D, Croft B, Hoffman J, Liu G, Stone H, Sullivan D (2006) Hypoxia: importance in tumor biology, noninvasive measurement by imaging, and value of its measurement in the management of cancer therapy *Int J Radiat Biol* **82**(10): 699–757

Tennant DA, Durán RV, Gottlieb E (2010) Targeting metabolic transformation for cancer therapy. *Nat Rev Cancer* **10**(4): 267–277

Tyagi RK, Azrad A, Degani H, Salomon Y (1996) Simultaneous extraction of cellular lipids and water-soluble metabolites: evaluation by NMR spectroscopy. *Magn Reson Med* **35**(2): 194–200

Vaupel P, Mayer A, Höckel M (2004) Tumor hypoxia and malignant progression. *Methods Enzymol* **381**: 335–354

Walker-Samuel S, Orton M, McPhail LD, Robinson SP (2009) Robust estimation of the apparent diffusion coefficient (ADC) in heterogeneous solid tumors. *Magn Reson Med* **62**(2): 420–429

Wang GL, Semenza GL (1995) Purification and characterization of hypoxia-inducible factor 1. *J Biol Chem* **270**(3): 1230–1237

Weihua Z, Tsan R, Huang WC, Wu Q, Chiu CH, Fidler IJ, Hung MC (2008) Survival of cancer cells is maintained by EGFR independent of its kinase activity. *Cancer Cell* **13**(5): 385–393

Welsh S, Williams R, Kirkpatrick L, Paine-Murrieta G, Powis G (2004) Antitumor activity and pharmacodynamic properties of PX-478, an inhibitor of hypoxia-inducible factor-1alpha. *Mol Cancer Ther* **3**(3): 233–244

Wise DR, DeBerardinis RJ, Mancuso A, Sayed N, Zhang XY, Pfeiffer HK, Nissim I, Daikhin E, Yudkoff M, McMahon SB, Thompson CB (2008) Myc regulates a transcriptional program that stimulates mitochondrial glutaminolysis and leads to glutamine addiction. *Proc Natl Acad Sci USA* **105**(48): 18782–18787

Workman P, Aboagye EO, Balkwill F, Balmain A, Bruder G, Chaplin DJ, Double JA, Everitt J, Farningham DA, Glennie MJ, Kelland LR, Robinson V, Stratford IJ, Tozer GM, Watson S, Wedge SR, Eccles SA (2010) Guidelines for the welfare and use of animals in cancer research *Br J Cancer* **102**(11): 1555–1577

Younes M, Brown RW, Stephenson M, Gondo M, Cagle PT (1997) Overexpression of Glut1 and Glut3 in stage I nonsmall cell lung carcinoma is associated with poor survival. *Cancer* **80**(6): 1046–1051

Zhao M, Pipe J, Bonnett J, Evelhoch J (1996) Early detection of treatment response by diffusion-weighted 1H-NMR spectroscopy in a murine tumour *in vivo. Br J Cancer* **73**(1): 61–64

Zhong H, De Marzo AM, Laughner E, Lim M, Hilton DA, Zagzag D, Buechler P, Isaacs WB, Semenza GL, Simons JW (1999) Overexpression of hypoxia-inducible factor 1alpha in common human cancers and their metastases. *Cancer Res* **59**(22): 5830–5835

Translational Therapeutics